



## Biochemical and structural characterization of 5'-methylthioadenosine nucleosidases from *Arabidopsis thaliana* ☆

Eun Young Park<sup>a</sup>, Woo Suk Choi<sup>a</sup>, Seung-Ick Oh<sup>a</sup>, Kyung-Nam Kim<sup>b</sup>, Jeong Sheop Shin<sup>a</sup>, Hyun Kyu Song<sup>a,\*</sup>

<sup>a</sup>School of Life Sciences and Biotechnology, Korea University, Anam-Dong, Seongbuk-Gu, Seoul 136-701, Republic of Korea

<sup>b</sup>Department of Molecular Biology, Sejong University, Seoul 143-747, Republic of Korea

### ARTICLE INFO

#### Article history:

Received 12 February 2009

Available online 26 February 2009

#### Keywords:

Adenine  
Crystal structure  
Flexible loop  
MTA  
Nucleosidase  
Plant  
SAH  
Spectroscopic assay

### ABSTRACT

5'-Methylthioadenosine (MTA) and S-adenosylhomocysteine (SAH) are important metabolites in all living organisms. Two similar nucleosidases for hydrolyzing MTA in *Arabidopsis thaliana* (AtMTAN1 and AtMTAN2) exist, but only AtMTAN2 shows markedly broad substrate specificity for hydrolysis of SAH. To examine the biochemical characteristics of AtMTAN2, it was over-expressed in *Escherichia coli* and purified to homogeneity. Spectroscopic assays confirm AtMTAN2 catalyzes MTA as well as SAH hydrolysis, compared to AtMTAN1 which only hydrolyzes MTA. In addition, crystal structure of the AtMTAN2 enzyme in complex with adenine was determined at 2.9 Å resolution. Finally, a structural comparison of AtMTAN2 performed with previously determined structures of AtMTAN1 and an *E. coli* homolog provides clues for the substrate specificity of MTA nucleosidases in *A. thaliana*.

© 2009 Elsevier Inc. All rights reserved.

### Introduction

Methylthioadenosine (MTA) and S-adenosylhomocysteine (SAH) are crucial metabolites amongst all living organisms, involved in biosynthetic pathways such as recycling of methionine (Met) and S-adenosyl-Met (AdoMet), protein and DNA methylation, and biosynthesis of ethylene, polyamines, and phytosiderophores [1,2]. The metabolism of MTA/SAH in a bacterial system has been studied extensively, including the identification and characterization of enzymes in the reaction pathways and the examination of reaction intermediates for potential development of antibiotics [3]. The MTA cycle in plants has also been well-characterized because of the synthesis of ethylene and polyamines, which play critical roles in plant physiology [4–6]. Several genes involved in the plant MTA cycle have recently been identified and characterized [5,7–10]. For example, MTA nucleosidase (MTAN) cleaves the ribosidic bond of MTA to produce the enzymatic products 5'-meth-

ylthioribose (MTR) and adenine [11]. MTR kinase then phosphorylates the C-1 hydroxyl group of the ribose moiety of MTR to yield MTR-1-phosphate [7,12]. Interestingly, generation of MTR-1-phosphate from MTA is a single-step reaction mediated by MTA phosphorylase (MTAP) in mammals [1,13].

Catabolism of SAH differs among species, however. Mammals use a separate enzyme, SAH hydrolase that cleaves the covalent bond between homocysteine and adenosine [14], whereas bacteria use MTA/SAH nucleosidase, which cleaves the same covalent bond between MTR and adenine in MTA as well as the bond between S-ribosylhomocysteine and adenine in SAH. Extensive biochemical and structural studies on MTA/SAH nucleosidase from *E. coli* (EcMTAN) have provided tremendous information concerning the catalytic mechanism, specific interactions with substrates, and conformational changes during the enzymatic reaction [13,15–19]. However, biochemical and structural studies on MTA nucleosidase from plants have been relatively limited in contrast to the bacterial enzyme. Previously, a biochemically and structurally characterization of an MTAN from *Arabidopsis thaliana* (AtMTAN1; AT4G38800) [20] showed AtMTAN1 hydrolyzes MTA and not SAH, in contrast to the bacterial enzyme which does. This result and the additional biochemical characterization of MTANs from *Lupinus luteus* seeds and *A. thaliana* (AtMTAN1) [11,20] demonstrate why plant MTAN has been known for specificity for MTA, but not for SAH. However, an MTAN from *Oryza sativa* L. possesses substantial hydrolytic ability of the ribosidic bond in SAH [5]. Another MTAN

**Abbreviations:** AdoMet, S-adenosyl-methionine; AtMTAN1, *Arabidopsis thaliana* MTAN1; AtMTAN2, *Arabidopsis thaliana* MTA/SAH nucleosidase; EcMTAN, *E. coli* MTA/SAH nucleosidase; MTAN, 5'-methylthioadenosine nucleosidase; MTAP, 5'-methylthioadenosine phosphorylase; MTR, 5'-methylthioribose; RMSD, root-mean square deviation; SAH, S-adenosylhomocysteine

\* The atomic coordinates and structure factors (ID code: 3BSF) have been deposited in the Protein Data Bank (<http://www.rcsb.org>).

\* Corresponding author. Fax: +82 2 3290 3628.

E-mail address: [hksong@korea.ac.kr](mailto:hksong@korea.ac.kr) (H.K. Song).

identified in the *Arabidopsis* genome (AtMTAN2; AT4G34840) was examined for its biochemical properties in recent study [21] and as well as this current one. Although sequence alignment between these two plant homologues shows a very high degree of sequence conservation among the residues in the active site (Fig. 1), only AtMTAN2 is able to cleave the ribosidic bond in both SAH and MTA, similar to the bacterial enzyme. In order to understand the substrate specificity between AtMTAN1 and AtMTAN2, we have determined the crystal structure of AtMTAN2 and compared the biochemical and structural characteristics among MTANs.

## Materials and methods

**Over-expression and purification.** The full-length AtMTAN1 (AT4G38800) and AtMTAN2 (AT4G34840) genes were isolated from *A. thaliana* cDNA using standard PCR techniques. The PCR products were then cloned into a pGEX-4T3 expression vector (GE Healthcare). Vectors were next transformed into BL21 (DE3) RIL (Novagen) for the over-expression of proteins corresponding to AtMTAN1 and AtMTAN2. The transformed cells were cultured in LB media with 50 µg/ml ampicillin at 37 °C until OD<sub>600</sub> = 0.6. AtMTAN1 and AtMTAN2 were next induced by the addition of 0.2 mM IPTG for 20 h at 22 and 18 °C, respectively. After induction, cells were harvested by centrifugation at 6000 rpm and resuspended in ice-cold phosphate-buffered saline in the presence of 1 mM PMSF. The resuspended cells corresponding to both AtMTAN1 and AtMTAN2 were disrupted by ultrasonication and subsequently subjected to identical purification procedures. Soluble fractions of cell lysates separated by centrifugation at 15,000 rpm

and 4 °C were applied to a glutathione column as the first purification step. In order to remove the N-terminal glutathione S-transferase (GST) tag, the eluent containing GST-AtMTAN fusion proteins was treated with human α-thrombin (10 NIH unit/1 mg fusion protein, Enzyme research Ltd.) at 18 °C for 12 h. The target protein was further purified by anion exchange chromatography (HiTrap Q Sepharose Fast Flow, GE health care) followed by gel filtration chromatography (Superose 12 GL 10/300, GE Healthcare).

**Enzymatic assay and kinetics.** MTA/SAH nucleosidase activities of both AtMTAN1 and AtMTAN2 were measured using SpectraMax M5 spectrophotometer (Molecular Devices, USA). Decreased absorbance at A<sub>275</sub> corresponding to the hydrolysis of the nucleoside was monitored and specific activities were calculated using the extinction coefficient for MTA hydrolysis ( $\epsilon_{275} = 1.6 \text{ mM}^{-1} \text{ cm}^{-1}$ ) [22]. Kinetic parameters were calculated in triplicate at 37 °C in 1 mL reactions containing 10–80 µM MTA and 50–300 µM SAH in 100 mM sodium phosphate buffer. Data for the Lineweaver-Burk in accordance with the Michaelis-Menton equation was performed by SigmaPlot.

**Crystallization and data collection.** The purified AtMTAN2 was concentrated to 7 mg/ml in 50 mM Tris-HCl (pH 8.0), 100 mM NaCl, and 1 mM DTT. Crystals were grown in sitting- and hanging-drop formations at 22 °C using equal volumes of protein and reservoir solutions. Initial crystallization conditions were obtained using multiple 96-well sitting-drop screens. After extensive optimization, crystals for data collection were grown in hanging-drop over a reservoir solution of 100 mM Bis-Tris (pH 6.5) and 26–32% (w/v) PEG-MME2000 within 3–5 days. Crystals were flash frozen and stored in liquid nitrogen with reservoir solution and 25%

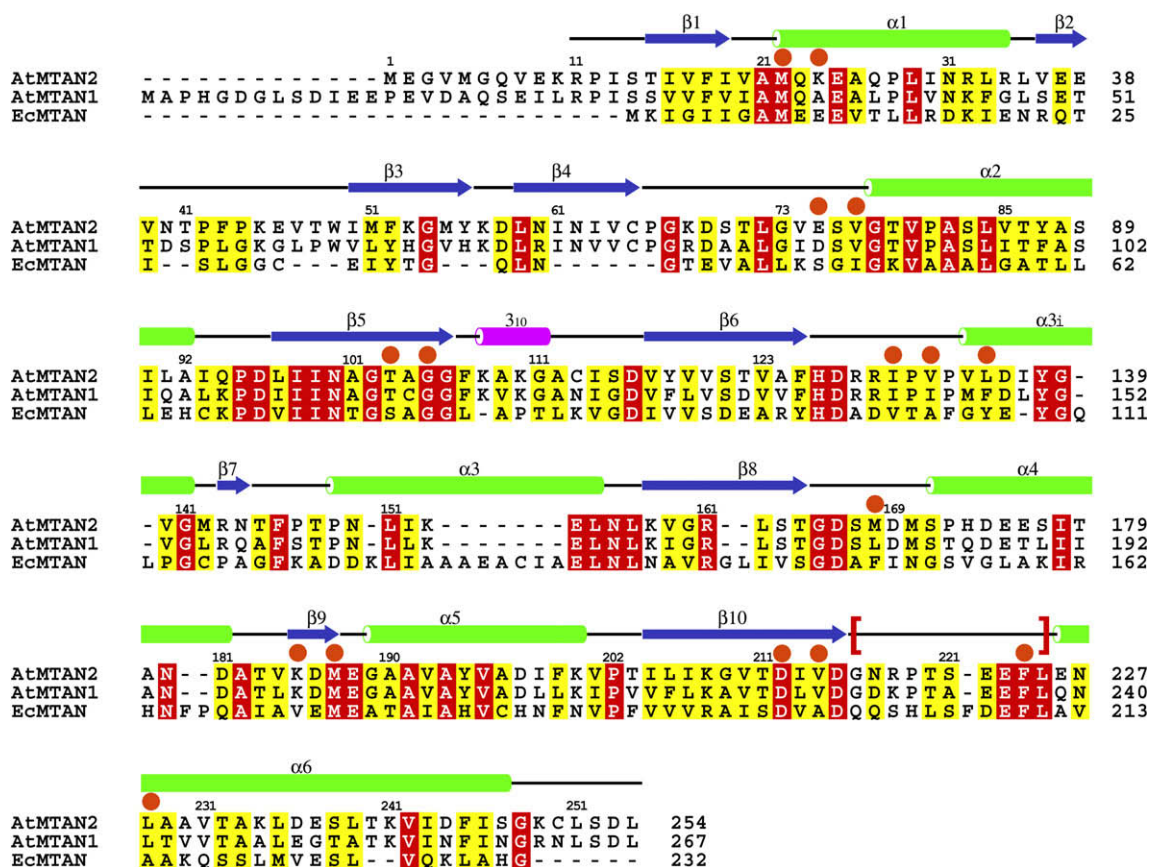


**Fig. 1.** Sequence alignment between AtNTAN1, AtMTAN2 and EcMTAN. The secondary structural elements at the top of each alignment correspond to those of AtMTAN2. Strictly conserved residues boxed in red and yellow indicate conservatively substituted residues. The residues involved in ligand binding are marked by a filled, orange circle. The flexible loop involved in the open-close structural transition is highlighted with red brackets [ ]. The figure was drawn using ALSICRIP [29]. (For interpretation of the references to color in this figure legend, the reader is referred to the web version of this paper.)

(v/v) PEG400 as a cryo-protectant. The native diffraction data were collected on a charge-coupled device detector at NW12 beamline of the Photon Factory, Tsukuba, Japan. The diffraction data were processed and scaled using the HKL2000 software package [23] and statistics for the data collection are described in Table 1.

**Structure determination and refinement.** The MOLREP program [24] was used to obtain phases with the model of AtMTAN1 (PDB ID: 2H8G). The model was rebuilt by the program O [25] and COOT [26] and was refined with CNS including the bulk solvent correction [27]. With the exception of the flexible loop regions, 2-fold non-crystallographic symmetry was tightly maintained during the entire refinement. Solvent molecules were added using model-phased difference-Fourier maps [27]. The electron density of adenine was unambiguously visible, even in the initial, molecular replacement-phased map. The AtMTAN2 crystals, however, were obtained in the absence of adenine. The assessment of model geometry and the assignment of secondary structural elements were obtained using the PROCHECK program [28]. Statistics for the refinement and model quality are described in Table 1. SAH coordinates were obtained from the protein data bank (PDB ID: 1HNN). The model of AtMTAN2 in complex with SAH was generated by finding the optimal fit for the active sites and further minimizing energy using the program CNS [27].

## Results and discussion

### Structure determination

Although previous knowledge recognizes AtMTANs and EcMTAN share limited sequence identity, both however show significant sequence conservation for the key residues involved in enzymatic catalysis (Fig. 1) [13,20,21]. The oligomeric state of AtMTAN1 and AtMTAN2 in solution was confirmed during gel filtration as a dimer, subsequently shown to be in the asymmetric unit of the present trigonal-crystal form of AtMTAN2. The crystals of AtM-

TAN2 were diffracted to an approximate resolution of 2.9 Å using a Synchrotron source (Table 1). The molecular replacement method using a highly refined AtMTAN1 model (PDB ID: 2H8G) was attempted to obtain phases. The structure of AtMTAN2 was refined to 2.9 Å resolution (Table 1) with the monomer consisting of seven  $\alpha$ -helices, ten  $\beta$ -strands, and a  $3_{10}$ -helix (Fig. 1). Similar to previous reports regarding AtMTAN1, the first 10 residues (Met1-Lys10) of AtMTAN2 were not observed in the electron density, implying disordered structure [20]. Residues between 216 and 225 in AtMTAN2 demonstrated weak electron density for both subunits, therefore indicating this loop has high flexibility. Interestingly, the equivalent segment in AtMTAN1 showed clear and strong electron density [20], whereas that in EcMTAN was not observed in the complex structure with adenine [18]. Bound adenine is located in the deep pocket formed by the monomer with the entrance partially covered by the adjacent subunit. This flap is critical in the formation of a wide dimer interface (Fig. 2A and B).

### Structural comparison of AtMTAN1 and AtMTAN2

Overall superposition of AtMTAN1 and AtMTAN2 performed with the program CNS [27] showed the residues between 216 and 225 in AtMTAN2 contain conformational differences representing an open conformation when compared with AtMTAN1 (Fig. 2A and B). Interestingly, AtMTAN1 (PDB ID: 2QSU) displayed a more open apo-form in this region compared with our AtMTAN2 structure (Fig. 2A and B) [21]. Superposition of C $\alpha$  atoms from AtMTAN2 with equivalent atoms from AtMTAN1 produced a root-mean square deviation (RMSD) less than 1.3 Å. If the largely deviated parts (>3 Å) are removed for comparison, the difference is further reduced to approximately 0.72 Å (Fig. 2C and D). In fact, the RMSD of the residues between 231 and 239 from AtMTAN1, which correspond the residues between 218 and 226 in AtMTAN2, is more than 5 Å (Fig. 2B).

Recent research found this region within the adenine-free form of AtMTAN1 exists as two distinct formations [21]. In fact, the equivalent monomer chains belonging to the adenine-free and -bound forms of AtMTAN1 produced RMSD results of 2.03 Å for open and 0.82 Å for closed forms. These results imply adenine-bound AtMTAN1 is shown exclusively in its closed form and moreover substantial conformational changes occur in this region during the enzymatic reaction. In addition, the RMSD (between 1.58 and 1.64 Å) of matching C $\alpha$  atoms between AtMTAN1 and AtMTAN2 monomers confirms AtMTAN2 exists in a more open conformation compared with the closed structure observed in adenine-bound AtMTAN1 (Fig. 2B).

### Active sites

AtMTAN1 and AtMTAN2 are very well superimposed with many active site residues demonstrating an invariant relationship. Indeed, sequence alignment confirms the adenine binding sites of AtMTAN1 and AtMTAN2 are well conserved (Fig. 1). Although the resolution of AtMTAN2 structure is lower than that of AtMTAN1 (1.5 Å vs 2.9 Å), the adenine molecule in the active site of AtMTAN2 is very clearly defined.

The side chains Met22, Val78, Met168, Met188, Phe224 along with Ile130', Val132' and Leu135' (for clarity we use "prime (')") to designate residue in one of the two subunits) in a neighboring AtMTAN2 monomer bind adenine via hydrophobic and van der Waals interactions similar to the corresponding residues of AtMTAN1 (Met35, Val90, Leu181, Met201, Phe237 and Ile143', Ile145', Phe148') (Fig. 3) [20]. The two noticeable hydrophobic side chains, Phe224 in AtMTAN2 (Phe237 in AtMTAN1) and Met168 in AtMTAN2 (Leu181 in AtMTAN1), show structural perturbations that provide the flexible accommodation of the adenine ring. The car-

**Table 1**  
Data collection and refinement statistics.

	AtMTAN2
<i>Data collection</i>	
Space group	P3 <sub>1</sub> 21
<i>Cell parameters</i>	
a, b, c (Å)	79.349, 79.349, 138.152
$\alpha$ , $\beta$ , $\gamma$ (°)	90, 90, 120
Wavelength (Å)	1.0000
Resolution (Å)	2.9 (2.9–3.02) <sup>a</sup>
R <sub>merge</sub> <sup>b</sup>	9.9 (56.5)
I/(I)	30.96 (5.35)
Total reflections	105,554
Unique reflections	11,186
Completeness (%)	96.5 (100)
<i>Refinement</i>	
Resolution range	50–2.9
Reflections used	10,250
R-factor/R <sub>free</sub> <sup>c</sup> (%)	25.3/29.3
Number of atoms	
Protein	3,700
Water/adenine	23/20
<i>RMS deviations</i> <sup>d</sup>	
Bond length (Å)	0.009
Bond angles (°)	1.34
Ramachandran outlier	0

<sup>a</sup> Values in parentheses are for reflections in the highest resolution bin.

<sup>b</sup>  $R_{\text{merge}} = \sum_h \sum_i |I(h,i) - \langle I(h) \rangle| / \sum_h \sum_i I(h,i)$ , where  $I(h,i)$  is the intensity of the  $i$ th measurement of reflection  $h$  and  $\langle I(h) \rangle$  is the corresponding average value for all  $i$  measurements.

<sup>c</sup>  $R = \sum ||F_o| - |F_c|| / \sum |F_o|$ , where  $R_{\text{free}}$  is calculated for the 10% test set of reflections.

<sup>d</sup> RMS, Root-mean square.

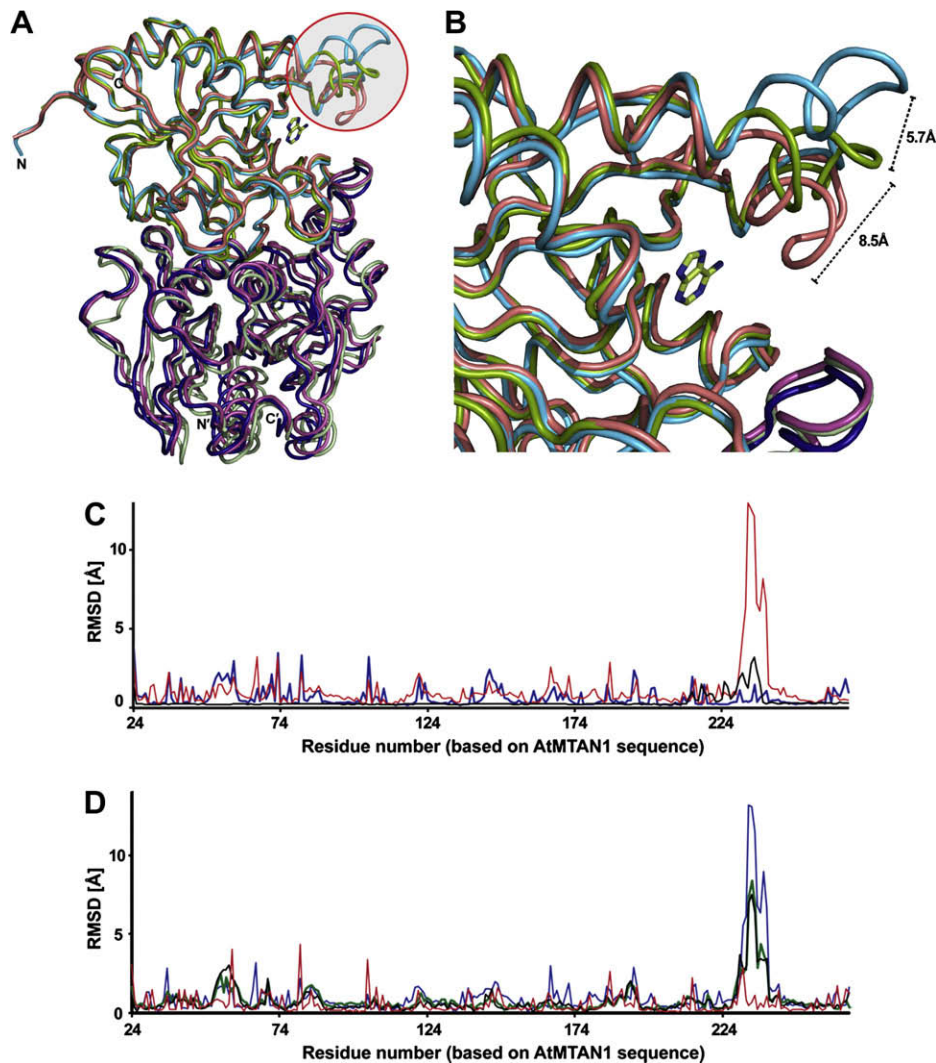


**Fig. 2.** Superposition of AtMTAN1 and AtMTAN2. (A) Backbone superposition of free (cyan), adenine-bound form (salmon) of AtMTAN1, and adenine-bound form (green) of AtMTAN2. The region showing significant structural movement ( $>3$  Å RMSD) is marked with a red circle. (B) Close-up view of the red circle marked in panel (A). The maximal shifts from the adenine-bound AtMTAN2 are indicated. (C) Plot of the difference between the chains belonging to the AtMTAN1 and AtMTAN2 dimers (red line—free AtMTAN1, blue line—adenine-bound form of AtMTAN1, black line—adenine-bound form of AtMTAN2). (D) Comparison between equivalent chains from AtMTAN1 and AtMTAN2 (blue line—A chain of AtMTAN1 between adenine-bound and free form, red line—B chain of AtMTAN1 between adenine-bound and free form, green line—A chain of adenine-bound form between AtMTAN1 and AtMTAN2, black line—B chain of adenine-bound form between AtMTAN1 and AtMTAN2). The RMSD for the main chain atoms of each residue are plotted as a function of AtMTAN1 residue number. (For interpretation of the references to color in this figure legend, the reader is referred to the web version of this paper.)

boxylic side chain of Asp211 in AtMTAN2 (Asp225 in AtMTAN1) hydrogen bonds with nitrogen atoms in the adenine ring, therefore being key determinants for the adenine base. The side chain Thr103 in AtMTAN2 (Thr116 in AtMTAN1) and backbone Gly105 in AtMTAN2 (Gly118 in AtMTAN1) also interact with the adenine molecule (Fig. 3B and C).

Interesting features can be derived from the SAH model when fit into the active site of AtMTAN1 and AtMTAN2 (Fig. 3E and F). For example, Phe148' in AtMTAN1 is substituted for Leu135' in AtMTAN2. The protruding Phe148' in AtMTAN1 may clash with the carboxyl group of SAH due to the bulkiness of both protruding phenolic ring of Phe148' and the carboxylic end of the homocysteine moiety. This is usually interpreted as AtMTAN1 being able to hydrolyze smaller 5'-methyl, 5'-ethyl, 5'-*n*-butyl, and 5'-isobutylthioadenosine, but not SAH [11]. Furthermore, this collision involving Phe148' is predictable when compared with adenine-free AtMTAN1, even though it has more opened conformation [21]. Therefore, the SAH model demonstrates the substitution of this po-

sition in AtMTAN2 results in the dual activity of MTA and SAH (Figs. 3E, F and 4A). In addition, Ile145' in AtMTAN1 is substituted to Val132' in AtMTAN2 (Fig. 4B). The removal of a methyl moiety from this residue may contribute to the favorable bonding with SAH. Lys24 and Glu75 in AtMTAN2 are located nearby SAH whereupon their side chains interact with SAH (Fig. 4B).

#### Enzyme activities

Although both AtMTAN1 and AtMTAN2 are able to convert MTA to MTR and adenine, only AtMTAN2 is able to do so with SAH (Fig. 4A). AtMTAN2 clearly possesses SAH hydrolysis activity, which itself remains unpredictable due to its 67% sequence identity with AtMTAN1 (Fig. 1). Although its sequence identity with EcMTAN is only 25% (Fig. 1), AtMTAN2 shows higher functional similarity with EcMTAN than AtMTAN1. Concerning catalysis, hydrolysis of MTA seems to predominate despite AtMTAN2 possessing both MTA and SAH hydrolysis activity (Fig. 4A). The  $K_M$  val-

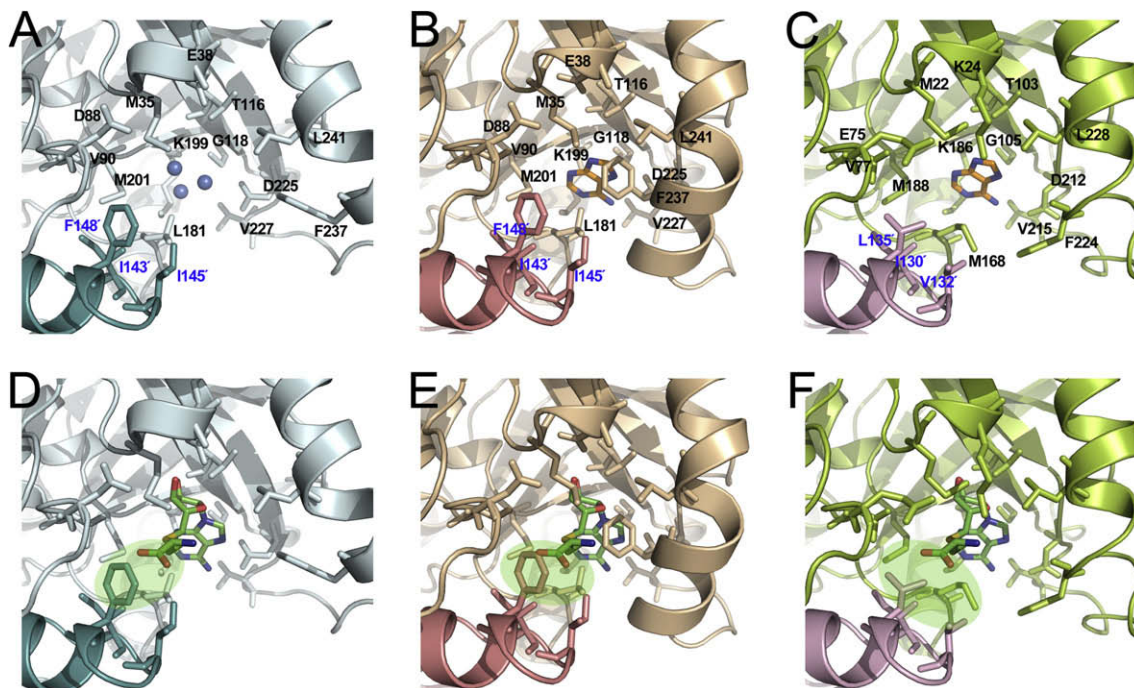


**Fig. 3.** Close-up view of the active sites in AtMTAN1 and AtMTAN2. The details of the active sites in free (A) and adenine-bound (B) AtMTAN1. Blue spheres indicate water molecules. (C) The active site of AtMTAN2 with bound adenine. Blue labels indicate residues that are originated from a different subunit. The modeled SAH fit into the active site in free (D) and adenine-bound (E) AtMTAN1, and adenine-bound AtMTAN2 (F). The green-colored, transparent ovals represent steric clashes between the phenolic ring of AtMTAN1 and the carboxyl group of SAH (D,E). (F) Leucine residue in AtMTAN2, aligned with F237 in AtMTAN1, shows no steric clash with the carboxyl group of SAH. (For interpretation of the references to color in this figure legend, the reader is referred to the web version of this paper.)

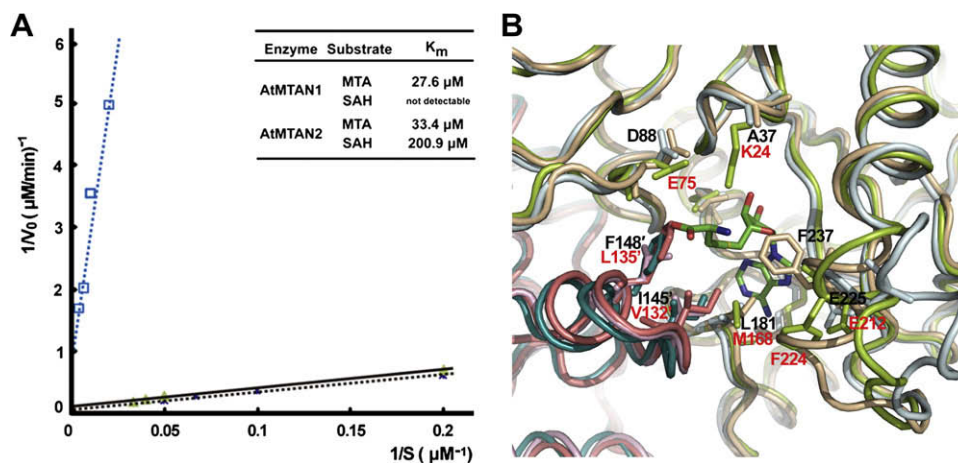


**Fig. 4.** (A) Double reciprocal plot of AtMTAN1 and AtMTAN2 for MTA and SAH. Solid (—) and dashed black line (----) show the MTA hydrolysis activity of AtMTAN1 and AtMTAN2, respectively. Dashed blue line with squares (---□---) represents SAH hydrolysis activity of AtMTAN2. SAH hydrolysis in AtMTAN1 was not detectable. (B) Conformational changes in the active site of AtMTAN1 and AtMTAN2. Superposition among free AtMTAN1 and adenine-bound AtMTAN1 and AtMTAN2 (Color coding is the same as Fig. 3). Black labels indicate residues of AtMTAN1 while red are those of AtMTAN2. (For interpretation of the references to color in this figure legend, the reader is referred to the web version of this paper.)

ues for MTA from both AtMTAN1 and AtMTAN2 are very similar in range. However, the  $K_m$  value for SAH is only 16.6% of MTA, meaning AtMTAN2 binds MTA approximately 6-fold higher than SAH (Fig. 4A). Intriguingly, this is consistent with previous reports that the maximum activity for hydrolysis of SAH by MTAN from rice is only 15.9%, when using MTA hydrolysis as a 100% standard [5]. Compared with bacterial MTAN [17], AtMTAN2 demonstrates similar substrate specificity and lower catalytic power. Although further structural information on the AtMTAN2 and SAH complex is needed, this report suggests subtle differences in the active site shown in Figure 4B in addition to the flexibility of the loop between 216 and 225 (compared to the conformational rigidity of

that loop in AtMTAN1) account for the broad substrate specificity of AtMTAN2 in the hydrolysis of SAH and MTA.

#### Acknowledgments

We thank the staff at 4A beamline, Pohang Light Source, Korea and NW12 beamline, Photon Factory, Japan for helping with the data collection. This work was supported by grants from the Plant Signaling Network Research Center and Molecular and Cellular Biodiscovery Research Program (M10648230002-08N4823-00210), Korea Science and Engineering Foundation.

## References

- [1] F. Schlenk, Methylthioadenosine, *Adv. Enzymol. Relat. Areas Mol. Biol.* 54 (1983) 195–265.
- [2] P.K. Chiang, R.K. Gordon, J. Tal, G.C. Zeng, B.P. Doctor, K. Pardhasaradhi, P.P. McCann, S-adenosylmethionine and methylation, *FASEB J.* 10 (1996) 471–480.
- [3] A. Sekowska, A. Danchin, The methionine salvage pathway in bacillus subtilis, *BMC Microbiol.* 2 (2002) 8.
- [4] J.H. Miyazaki, S.F. Yang, The methionine salvage pathways in relation to ethylene and polyamine biosynthesis, *Physiol. Plant* 69 (1987) 366–370.
- [5] G. Rzewuski, K.A. Cornell, L. Rooney, K. Burstenbinder, M. Wirtz, R. Hell, M. Sauter, OsMTN encodes a 5'-methylthioadenosine nucleosidase that is up-regulated during submergence-induced ethylene synthesis in rice (*Oryza sativa* L.), *J. Exp. Bot.* 58 (2007) 1505–1514.
- [6] M.M. Kushad, G. Yelenosky, R. Knight, Interrelationship of polyamine and ethylene biosynthesis during avocado fruit development and ripening, *Plant Physiol.* 87 (1988) 463–467.
- [7] M. Sauter, K.A. Cornell, S. Beszteri, G. Rzewuski, Functional analysis of methylthioribose kinase genes in plants, *Plant Physiol.* 136 (2004) 4061–4071.
- [8] S.O. Yoon, Y.S. Lee, S.H. Lee, Y.D. Cho, Polyamine synthesis in plants: isolation and characterization of spermidine synthase from soybean (*glycine max*) axes, *Biochim. Biophys. Acta* 1475 (2000) 17–26.
- [9] X. Good, J.A. Kellogg, W. Wagoner, D. Langhoff, W. Matsumura, R.K. Bestwick, Reduced ethylene synthesis by transgenic tomatoes expressing S-adenosylmethionine hydrolase, *Plant Mol. Biol.* 26 (1994) 781–790.
- [10] M.M. Kushad, D.G. Richardson, A.J. Ferro, 5'-methylthioadenosine nucleosidase and 5-methylthioribose kinase activities and ethylene production during tomato fruit development and ripening, *Plant Physiol.* 79 (1985) 525–529.
- [11] A.B. Guranowski, P.K. Chiang, G.L. Cantoni, 5'-methylthioadenosine nucleosidase. Purification and characterization of the enzyme from *Lupinus luteus* seeds, *Eur. J. Biochem.* 114 (1981) 293–299.
- [12] M.M. Kushad, D.G. Richardson, A.J. Ferro, 5-methylthioribose kinase activity in plants, *Biochem. Biophys. Res. Commun.* 108 (1982) 167–173.
- [13] J.E. Lee, E.C. Settembre, K.A. Cornell, M.K. Riscoe, J.R. Sufrin, S.E. Ealick, P.L. Howell, Structural comparison of MTA phosphorylase and MTA/AdoHcy nucleosidase explains substrate preferences and identifies regions exploitable for inhibitor design, *Biochemistry* 43 (2004) 5159–5169.
- [14] M.A. Turner, X. Yang, D. Yin, K. Kuczera, R.T. Borchardt, P.L. Howell, Structure and function of S-adenosylhomocysteine hydrolase, *Cell Biochem. Biophys.* 33 (2000) 101–125.
- [15] J.E. Lee, W. Luong, D.J. Huang, K.A. Cornell, M.K. Riscoe, P.L. Howell, Mutational analysis of a nucleosidase involved in quorum-sensing autoinducer-2 biosynthesis, *Biochemistry* 44 (2005) 11049–11057.
- [16] J.E. Lee, V. Singh, G.B. Evans, P.C. Tyler, R.H. Furneaux, K.A. Cornell, M.K. Riscoe, V.L. Schramm, P.L. Howell, Structural rationale for the affinity of pico- and femtomolar transition state analogues of *Escherichia coli* 5'-methylthioadenosine/S-adenosylhomocysteine nucleosidase, *J. Biol. Chem.* 280 (2005) 18274–18282.
- [17] J.E. Lee, G.D. Smith, C. Horvatin, D.J. Huang, K.A. Cornell, M.K. Riscoe, P.L. Howell, Structural snapshots of MTA/AdoHcy nucleosidase along the reaction coordinate provide insights into enzyme and nucleoside flexibility during catalysis, *J. Mol. Biol.* 352 (2005) 559–574.
- [18] J.E. Lee, K.A. Cornell, M.K. Riscoe, P.L. Howell, Structure of *E. coli* 5'-methylthioadenosine/S-adenosylhomocysteine nucleosidase reveals similarity to the purine nucleoside phosphorylases, *Structure* 9 (2001) 941–953.
- [19] J.E. Lee, K.A. Cornell, M.K. Riscoe, P.L. Howell, Structure of *Escherichia coli* 5'-methylthioadenosine/S-adenosylhomocysteine nucleosidase inhibitor complexes provide insight into the conformational changes required for substrate binding and catalysis, *J. Biol. Chem.* 278 (2003) 8761–8770.
- [20] E.Y. Park, S.I. Oh, M.J. Nam, J.S. Shin, K.N. Kim, H.K. Song, Crystal structure of 5'-methylthioadenosine nucleosidase from *Arabidopsis thaliana* at 1.5-Å resolution, *Proteins* 65 (2006) 519–523.
- [21] K.K. Siu, J.E. Lee, J.R. Sufrin, B.A. Moffatt, M. McMillan, K.A. Cornell, C. Isom, P.L. Howell, Molecular determinants of substrate specificity in plant 5'-methylthioadenosine nucleosidases, *J. Mol. Biol.* 378 (2008) 112–128.
- [22] V. Singh, J.E. Lee, S. Nunez, P.L. Howell, V.L. Schramm, Transition state structure of 5'-methylthioadenosine/S-adenosylhomocysteine nucleosidase from *Escherichia coli* and its similarity to transition state analogues, *Biochemistry* 44 (2005) 11647–11659.
- [23] Z. Otwinowski, W. Minor, Processing of X-ray diffraction data collected in oscillation mode, in: C.W. Carter, R.M. Sweet, (Eds.), *Methods Enzymology*, Academic Press, New York, 1997, pp. 307–326.
- [24] A. Vagin, A. Teplyakov, An approach to multi-copy search in molecular replacement, *Acta Crystallogr. D Biol. Crystallogr.* 56 Pt 12 (2000) 1622–1624.
- [25] T.A. Jones, J.-Y. Zou, S.W. Cowan, M. Kjeldgaard, Improved methods for binding protein models in electron density maps and the location of errors in these models, *Acta Crystallogr. A* 47 (1991) 110–119.
- [26] P. Emsley, K. Cowtan, Coot: model-building tools for molecular graphics, *Acta Crystallogr. D Biol. Crystallogr.* 60 (2004) 2126–2132.
- [27] A.T. Brunger, P.D. Adams, G.M. Clore, W.L. DeLano, P. Gros, R.W. Grosse-Kunstleve, J.S. Jiang, J. Kuszewski, M. Nilges, N.S. Pannu, R.J. Read, L.M. Rice, T. Simonson, G.L. Warren, Crystallography & nmr system: a new software suite for macromolecular structure determination, *Acta Crystallogr. D* 54 (1998) 905–921.
- [28] R. Laskowski, M. MacArthur, E. Hutchinson, J. Thornton, Procheck: a program to check the stereochemical quality of protein structures, *J. Appl. Crystallogr.* 26 (1993) 283–291.
- [29] G.J. Barton, ALSCRIPT: a tool to format multiple sequence alignments, *Protein Eng.* 6 (1993) 37–40.